IEEE Photonics Journal
An IEEE Photonics Society Publication

Open Access

Magneto-Refractive Effect and Mechanism Analysis of Erbium-Ytterbium Co-Doped Silica Fiber

Volume 13, Number 3, June 2021

Yanhua Dong
Caihong Huang
Wanting Sun
Sujuan Huang
Cheng Yan
Jianxiang Wen
Xiaobei Zhang
Yi Huang
Yana Shang
Heming Wei
Tingyun Wang

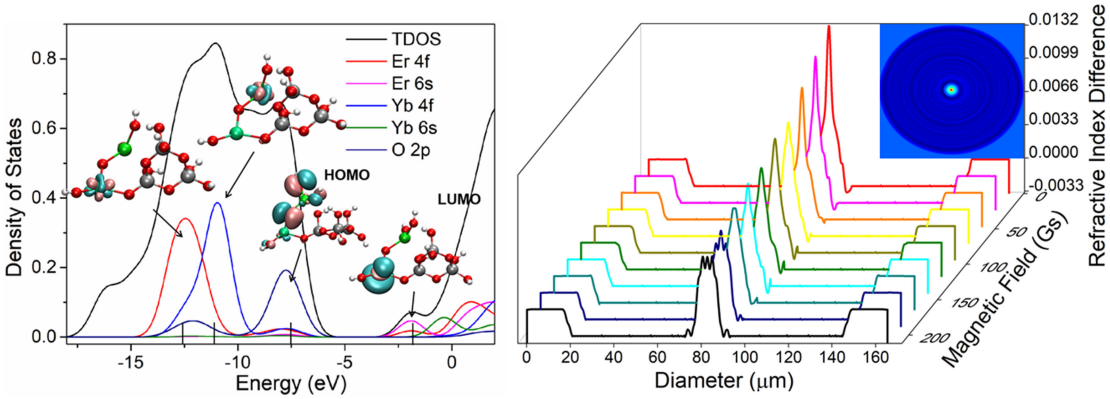

DOI: 10.1109/JPHOT.2021.3082163

Magneto-Refractive Effect and Mechanism Analysis of Erbium-Ytterbium Co-Doped Silica Fiber

Yanhua Dong, Caihong Huang, Wanting Sun, Sujuan Huang, Cheng Yan, Jianxiang Wen, Xiaobei Zhang, Yi Huang, Yana Shang, Heming Wei, and Tingyun Wang

Key Laboratory of Specialty Fiber Optics and Optical Access Networks, Joint International Research Laboratory of Specialty Fiber Optics and Advanced Communication, Shanghai University, Shanghai 200444, China

DOI:10.1109/JPHOT.2021.3082163

Manuscript received April 14, 2021; revised May 12, 2021; accepted May 17, 2021. Date of publication May 20, 2021; date of current version June 9, 2021. This work was supported in part by the Natural Science Foundation of China under Grants 61675125 and 61875118, and in part by 111 Project (D20031) and Shanghai professional technology platform (19DZ2294000). Corresponding author: Yanhua Dong (e-mail: dongyanhua@shu.edu.cn).

Abstract: The magneto-refractive properties of Er/Yb co-doped silica fiber (EYDF) are important in magnetic field sensing. Here, we proposed a theoretical calculation model of the EYDF using density functional theory (DFT) and demonstrated it by an interferometric digital hologram magneto-refractive measurement system. The calculation results show that the fiber material, doped with Er/Yb atoms, has a large net spin and asymmetric spin distribution, which enables the elements to play an important role in the magnetic characteristics of the material. The experimental results show that the refractive index of the fiber decreases linearly with the increase of the magnetic field. The sensitivity of EYDF is 3.8279×10^{-5} RIU/Gs and is two orders of magnitude higher than that of single-mode fiber which is confirmed by the theoretical calculation. It demonstrated that the EYDF has advantages and potential of high sensitivity, miniaturization, and easy integration for magnetic field detection in harsh environments.

Index Terms: Magneto-refractive effect, refractive index, Er/Yb co-doped silica fiber, density functional theory, digital holography.

1. Introduction

OPTICAL fiber magnetic field sensors have the advantages of strong anti-interference ability, good stability, and high sensitivity, which are widely used in geophysics, military guidance, and industrial inspections [1], [2]. At present, optical fiber magnetic field sensing methods mainly include the magneto-optic Faraday effect [3], tunable refractive index (RI) of magnetic fluid (MF) [4], and magnetostrictive method [5], etc. A magnetic field sensor based on the Faraday effect uses metallic glass and crystals with a large Verdet constant as the sensing unit to achieve target detection by measuring the Faraday rotation angle [6]. Although these sensors have the advantages of a simple structure and fast response speed, and are widely used in current and pulsed magnetic fields, there are certain drawbacks because the measurement of their optical path requires high polarization stability and their sensitivity is limited by the low Verdet constant. A magnetic field sensor based on MF uses the adjustable RI of the MF to the magnetic field strength

and direction [7]–[9]. Various new types of magnetic field sensors based on MF are currently being developed [10]; however, considerable advancements are required because MF has strong light absorption and is easily saturated. A magnetostrictive magnetic field sensor sticks to or coats a composite metal material on the surface of an optical fiber and grating as a probe, and measures the magnetic field by detecting the change in the phase of the optical fiber or wavelength of the grating [11]. Although these sensors have high sensitivity, precision, and are widely used in space magnetic field measurement, their stability is susceptible to the environment. Moreover, optical fiber magnetic field sensors combined with magnetic materials are unstable, and not suitable for use in complex and harsh environments such as underwater targets and high pressures. Thus, the development of a optic fiber magnetic sensor with high stability, fast response speed, and high sensitivity in high-performance sensing applications is highly essential. As a sensing unit, a doped fiber has significant advantages, such as easy network integration, high reliability, and the ability to function in complex environments. The magnetic susceptibility of rare-earth materials strongly depends on the magnetic field, and subtle changes cause changes in the RI of the optical fiber. Rare earth (RE) ions have abundant spin electrons, large spin magnetic moments, and high absolute energy level transitions, thus exhibiting abundant magnetic properties [12]. In addition, REs co-doped atoms provide more spin electrons, which can further enhance energy transfer, energy level matching, local coordination, and magneto-refractive effects [13]. Er^{3+} ion has a large number of unpaired 4f electrons, and there are a large number of electronic energy levels that can undergo photo-transition and splitting, which makes Er^{3+} ion possess rich magneto-optical properties [14]. The Erbium-doped fiber has the potential of high-sensitivity magneto-refractive properties, and the high doping concentration can improve the fiber sensitivity. However, the lack of sufficient coordination anions to bind to Er^{3+} in the preparation of optical fibers may result in uneven optical fiber distribution [15]. In addition, in the case of high doping concentration, concentration quenching may occur. The addition of Yb^{3+} ions can effectively inhibit the formation of Er^{3+} ions clusters and reduce the concentration of quenching. Additionally, the Yb^{3+} ions have strong magnetic properties of unpaired spin electrons as a sensitizing medium, which can increase signal gain, hence, the Er/Yb co-doped fiber is used as the gain medium.

In this study, the magneto-refractive effect of an EYDF was systematically examined. A theoretical model of the microscopic local structure of the EYDF material was established, and the spin magnetic moment, density of state, energy transfer and other characteristics of the model were calculated to examine the magneto-refractive mechanism. The composition and comprehensive magnetic properties of EYDF were experimentally investigated as well. Furthermore, using the digital holography technology, the refractive index change (RIC) of the optical fiber under the action of a magnetic field was measured and the results were compared with that of the single-mode fiber (SMF). The EYDF has the advantages of high sensitivity, simple structure, easy preparation, fast response speed, the viability of the Er/Yb co-doped optical fiber as a magnetic sensor was analyzed.

2. Theoretical Calculations

The magneto-refractive effect occurs when light passes through a magnetic material with a dielectric constant tensor. Under an external magnetic field, the magnetic susceptibility of the material changes, which affects the transmission state of the light passing through it. This results in a change in the dielectric tensor, which further changes the RI. The relationship between the RI n, the dielectric constant ε of the fiber, and the magnetic susceptibility χ is as follows [16]:

$$n = \sqrt{\varepsilon} = \sqrt{1 + 4\pi\chi} \tag{1}$$

The magnetic susceptibility is related to the magnetic moment, and the relationship between magnetic susceptibility and effective magnetic moment μ_{eff} in Bohr magnetons B.M can be

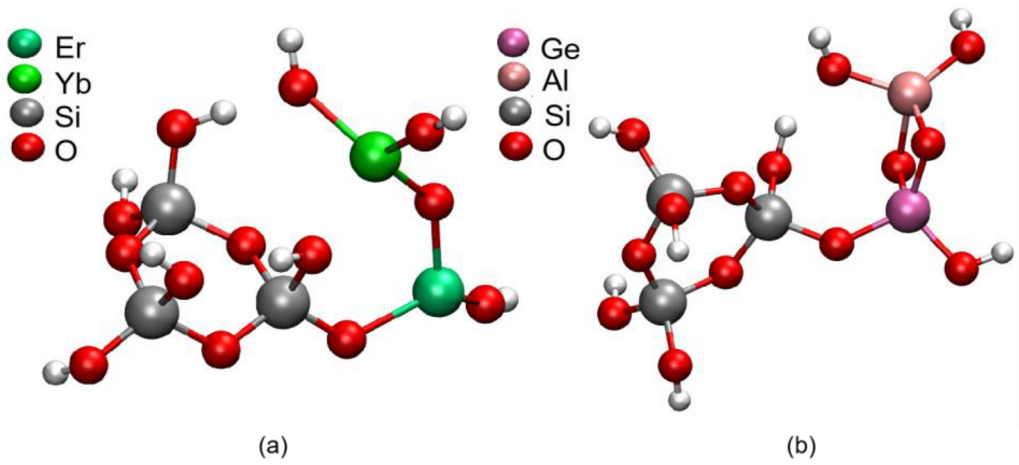

Fig. 1. (a) EYDF-3MR model. (b) GADF-3MR model.

described by the following relationship [17]:

$$\mu_{\text{eff}} = \sqrt{\frac{3k_B\chi T}{N_A\mu_B}}B \cdot M \tag{2}$$

where k_B is the Boltzmann constant, N_A is Avogadro number, T is the temperature (K), μ_B is the Bohr magneton. The magnetic moment is determined by the spin electrons; therefore, the spin-electron interaction of the material regulates the change in the RI of the fiber. Thus, the magneto-refractive properties of the fiber are obtained from the microscopic behavior of spin electrons.

Here, we used a relativistic effective core potential (RECP) to account for relativistic effects [18]. The B3LYP method of DFT was used to optimize the model of the Er/Yb co-doped silica three-ring fiber materials. Considering factors such as computing resources and accuracy, the 6-31G$*$ basis was used for oxygen, hydrogen, and silicon elements. The small-core pseudopotential basis ECPMWB28 with 28 core electrons was chosen for the Er and Yb atoms [19]. To demonstrate that the magnetic properties of the optical fiber were caused by the doping of rare-earth ions rather than the material of the fiber, an SMF model was investigated for comparison. In the SMF model, the 6-31G$*$ group was used for oxygen, hydrogen, silicon, and germanium elements [20]. The geometric structure optimization, energy calculation, and electronic structure were calculated using Gaussian 09 [21], and the electronic, optical characteristics, and spin characteristics and atomic interaction of the Er/Yb co-doped fiber were determined using Multiwfn [22].

2.1 Geometric Structures

The silica optical fiber model is generally composed of SiO_4 tetrahedral units and silicon dioxide irregular rings; in n-membered-rings (nMR), n denotes the number of Si atoms in the rings [23]. A 3MR microstructure model is suitable and widely accepted for use as a doped amorphous silica matrix [24]. The established model of the Er/Yb co-doped 3MR fiber materials (EYDF-3MR) shown in Fig. 1(a) is more stable and consistent with the experimental results [13]. For comparison, a model of Ge/Al co-doped 3MR fiber materials (GADF-3MR) is established as shown in Fig. 1(b). The parameters of the fiber materials model are listed in Table I, and were found to be close to the typical values [25], [26].

2.2 Electronic Structures

The energy of the models was calculated with different spin multiplicities M (M = 1, 3, 5, ...). The quintuplet state of the EYDF-3MR model was is the lowest; thus, the ground states were

TABLE I
Bond Length and Angle of the Models

Average bond length (Å)			Average bond angle (°)		
Er-O	Yb-O	Si-O	O-Er-O	O-Yb-O	O-Si-O
2.05	2.05	1.65	117.51	116.42	108.55

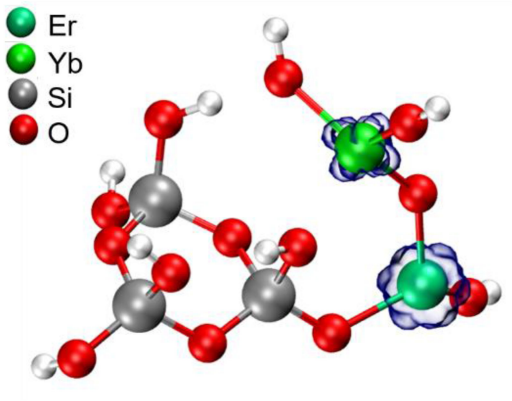

Fig. 2. Spin density distributions of EYDF-3MR.

quintet. The contributions to the electronic states of the system were obtained through spin density analysis. Fig. 2 shows the ground-state spin density of the EYDF-3MR model. The quintet spin state was attributed to the ferromagnetic coupling between the net spin electrons of the Er/Yb atoms and 3MR, with the Er/Yb atoms contributing more significantly. Further analysis on the spin density revealed that the number of net spin electrons in the Er and Yb atoms was $+2.99$ e and $+0.98$ e [27], respectively, whereas in 3MR, it is $+0.02$ e. Most electrons were concentrated in the O atoms that bonded with Er nearby. Therefore, the total number of spin electrons in the EYDF-3MR structure was approximately $+4.00$ e, thereby resulting in the quintet ground electronic state. From the spin density, we could clearly determine where the spin electrons were mainly distributed. Moreover, the contribution to the total magnetic moment m due to electron spin. If the spin population of a region is x, then its contribution to m would be x μ_{B} (Bohr magneton) [22]. The spin population of Er was $+2.99$ e, then magnetic moment m was 2.99 μ_{B}, in which the 4f orbital contribution was 2.95 μ_{B}. The ground state of the GADF-3MR structure is singlet, the spin electrons were arranged in opposite spins. In comparison with GADF, the magnetism of EYDF, originating from the contribution of rare-earth atoms, was stronger.

The electronic density and charge density distribution clearly reveal the charge movement and direction of bonding polarity in the coupling of bonding electrons [28]. Fig. 3(a) shows the electron density in the EYDF-3MR structure. There is a noticeable aggregation of electrons around the Er and O atoms. In Fig. 3(b), the solid line of the charge density distribution indicates charge accumulation, and the dotted line indicates charge depletion. As shown in Fig. 3(a) and Fig. 3(b), there is a significant electron accumulation between the Er atom and 3MR, which indicates the presence of valence interactions. The following analysis of the density of states and molecular orbital properties supports this conclusion.

2.3 Analysis of the Density of States

The density of states (DOS) of the EYDF-3MR and GADF-3MR structures are showing in Fig. 4, where the upper and lower parts represent the DOS of the alpha spin electrons and beta spin

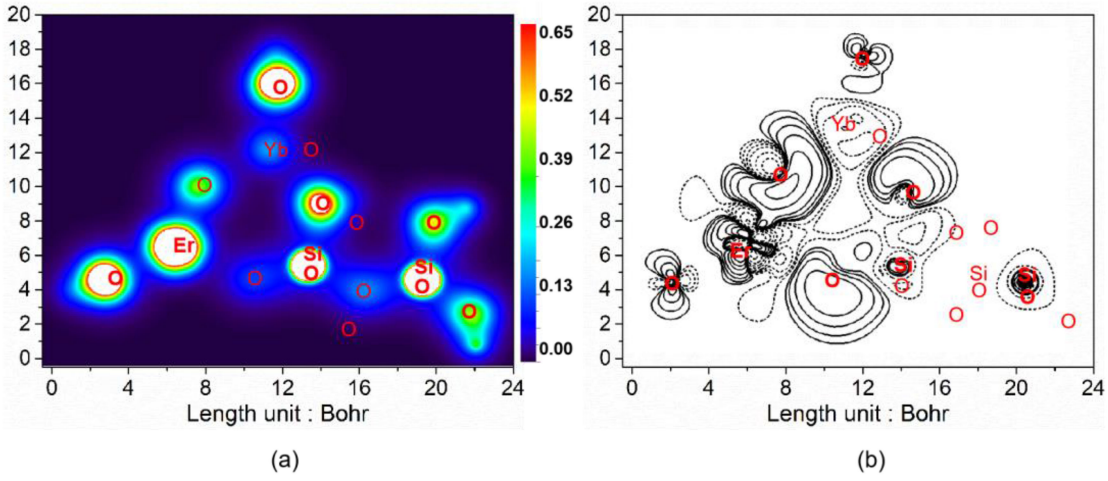

Fig. 3. (a) Electron density distributions of EYDF-3MR. (b) Charge density deformation of EYDF-3MR.

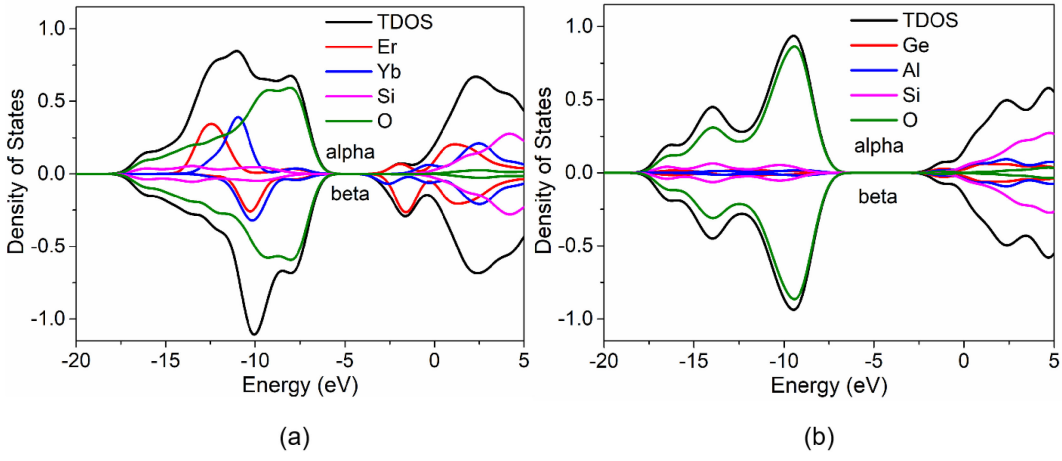

Fig. 4. Density of states of (a) EYDF-3MR and (b) GADF-3MR. The upper half represents the DOS of the alpha electrons, and the lower part represents the DOS of the beta electrons.

electrons, respectively. Fig. 4 shows that the difference between the alpha and beta values of the EYDF-3MR structure is larger than that of the alpha and beta values of the GADF-3MR structure. The DOS of the α and β electrons was not symmetric, which led to an obvious spin polarization carried by EYDF-3MF. This indicates that in the model of the optical fiber microstructure, the 3MR is more affected by the Er/Yb atoms, even with a changed energy level, thereby resulting in a strong bonding effect between them.

To further investigate the micro-mechanism of EYDF, we studied the interaction between the Er, Yb, and O atoms. It can be seen from Fig. 5 that the 4f orbitals of the Er and Yb atoms occupied the majority of the total density of states (TDOS), that is, the spin magnetic moment was mainly provided by the 4f orbital, and the main contribution of molecular magnetism was also from the 4f orbital of Er and Yb. Furthermore, the outer electrons in the 2p of O almost coincided with the TDOS of oxygen, and the main contribution of the interaction of the O atom was 2p orbital. The DOS distribution near the Fermi level (-7 eV) shows that the 2p orbital of the O atom overlaps with the 6s orbital of the Er and Yb atoms, and that there was an interaction between the 4f electrons of Er and Yb atoms, and the 2p electrons of O atoms.

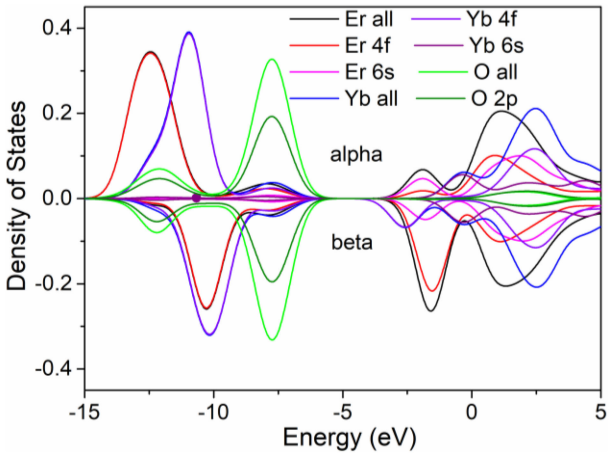

Fig. 5. Density of states of erbium, ytterbium, and oxygen.

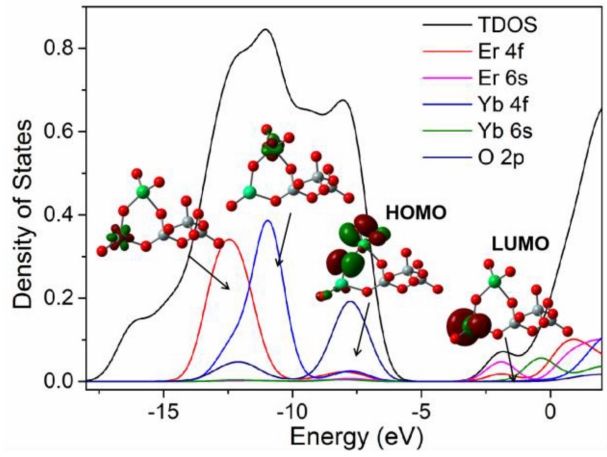

Fig. 6. The frontier molecular orbitals(spin-up) of the model of EYDF. Isovalue = 0.005.

Table II
Results of NAO Analysis of Frontier Molecular Orbitals

Orb	Er total	Yb total	O outer	O inner
HOMO-2	1.41%	5.38%	91.81%	1.08%
HOMO-1	3.85%	2.80%	92.00%	0.54%
HOMO	2.91%	4.09%	90.20%	2.00%
LUMO	83.62%	4.31%	-	0.50%

2.4 Molecular Orbitals Analysis

To quantitatively analyze the contribution from the frontier molecular orbitals, we calculated the contribution from the frontier molecular orbitals by using natural atomic orbitals (NAO) [29]. The DOS of the alpha and beta electrons were not symmetrical near the Fermi level, inducing obvious spin polarization induced by the Er/Yb atom. The O outer is the oxygen atoms around Er/Yb atoms, and the O inner is the oxygen atoms around the 3MR network. The 6s electrons of Er and Yb atoms are simultaneously donated to oxygen. The frontier molecular orbitals in Fig. 6 and Table II show that the orbitals of the Er/Yb atoms and 3MR contribute to the molecular orbitals of the system at a certain energy level. Additionally, these orbitals overlapped, which further revealed their interaction.

Table III
Weight Percentage List of the Er/Yb Co-Doped Silica Fibers

Elements	wt %
O	51.8
Si	45.7
Al	0.9
Ge	0.7
Er	0.7
Yb	0.2

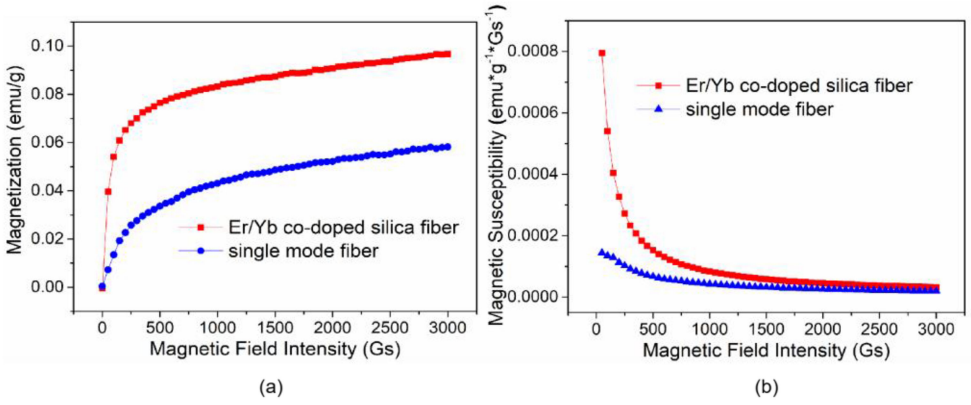

Fig. 7. The dependence of the magnetization (a) and magnetic susceptibility (b)on the magnetic field for EYDF and SMF at 300 K.

The density of states and frontier molecular orbitals indicated that there was a strong covalent interaction between the 4f electrons of Er/Yb and the 2p electrons of O around Er/Yb. Compared with the SMF, the EYDF had more spin electrons and a larger magnetic moment, and its energy level showed significant splitting. Under the action of an external magnetic field, the spin electrons were easily polarized and have abundant energy level transitions. Correspondingly, the magnetic susceptibility of the material was extremely easy to change, which was manifested externally as a change in the RI.

3. Experiment and Results

An EYDF was fabricated using a combined technology of modified chemical vapor deposition and atomic layer deposition [13]. The composition of the fiber was determined using Energy Dispersive Spectrometer (EDS) (OXFORD, England) and listed in Table III. The percentages of Er, Yb, and Al were 0.7, 0.2, and 0.9 wt%, respectively. A small amount of Al could improve the performance of the fiber, and the vintage concentration ratio remains to be explored.

The field-dependent magnetization of the EYDF was measured and characterized using a physical property measurement system (PPMS-9, Quantum Design, USA). The magnetization change of EYDF was greater than that of SMF, and its magnetic susceptibility curve was steeper, as shown in Fig. 7. With an increase in the magnetic field, the magnetization (magnetic moment) of the EYDF fiber increased, the magnetic susceptibility decreased, and the magnetic response characteristics of the magnetic field below 500 Gs became more significant.

The measurement system of the optical fiber RIC in our work was constructed based on the digital hologram technique [30], [31], as shown in Fig. 8. The system was composed of the transmission interference optical system of Mach-Zehnder, which records the digital hologram, and

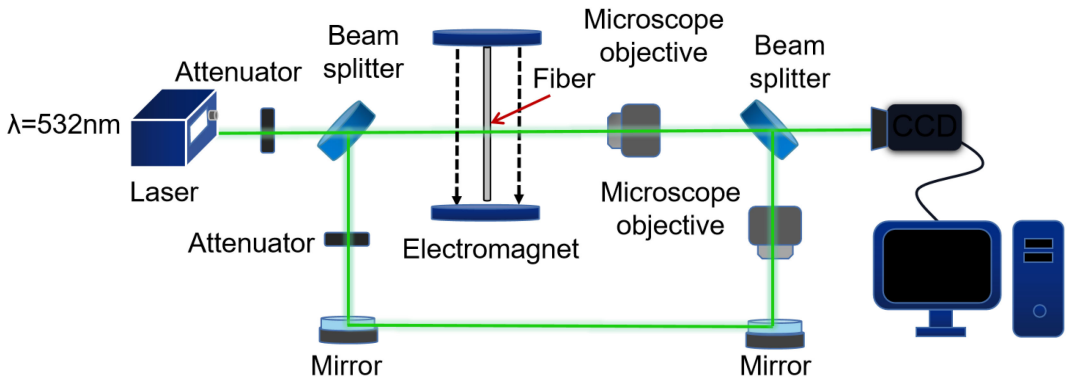

Fig. 8. Schematic of the magneto-refractive measurement system of digital holography of the optical fiber.

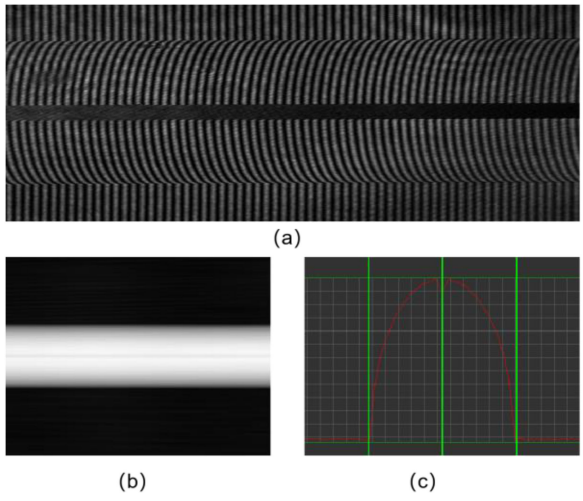

Fig. 9. Experimental results of EYDF: (a) the hologram of the fiber; (b) two-dimensional phase distribution of experimental hologram; (c) one-dimensional phase distribution of experimental hologram.

then the computer reproduces the RI of the optical fiber. The accuracy of the measurement of the RI of the optical fiber can reach 1×10^{-4}.

The interferometric digital hologram recorded by the CCD is shown in Fig. 9(a). Image processing and angular spectrum algorithms are performed to reconstruct the optical path information to obtain the phase [29], and the one-dimensional phase distribution curve and the two-dimensional phase distribution curve of the fiber were obtained by demodulation, as shown in Fig. 9(b) and Fig. 9(c). Then, the phase distribution is projected and integrated to obtain the two-dimensional and three-dimensional RI of the fiber as shown in Fig. 10 (a) and Fig. 10 (b). The core and cladding diameters were 9.52 μm and 120.66 μm, respectively, and the RI difference between core and cladding was 0.0138. Then, the optical fiber is placed in the center of the uniform magnetic field, and the magnetic field was changed by adjusting the electromagnet. We studied the optical fiber magneto-refractive properties, as shown in Fig. 11.

As the magnetic field increased, the RI of the cladding did not change significantly, whereas the RI of the core showed a linear decrease. The RI distribution of core becomes wider and the peak decreases sharply shown in Fig. 12(a). To analyze the magneto-refractive characteristics of EYDF, the magnetic field dependence of the core RI is calculated, as shown in Fig. 12(b), where the black and red curves represent the RIC of the EYDF and SMF, respectively. As the magnetic

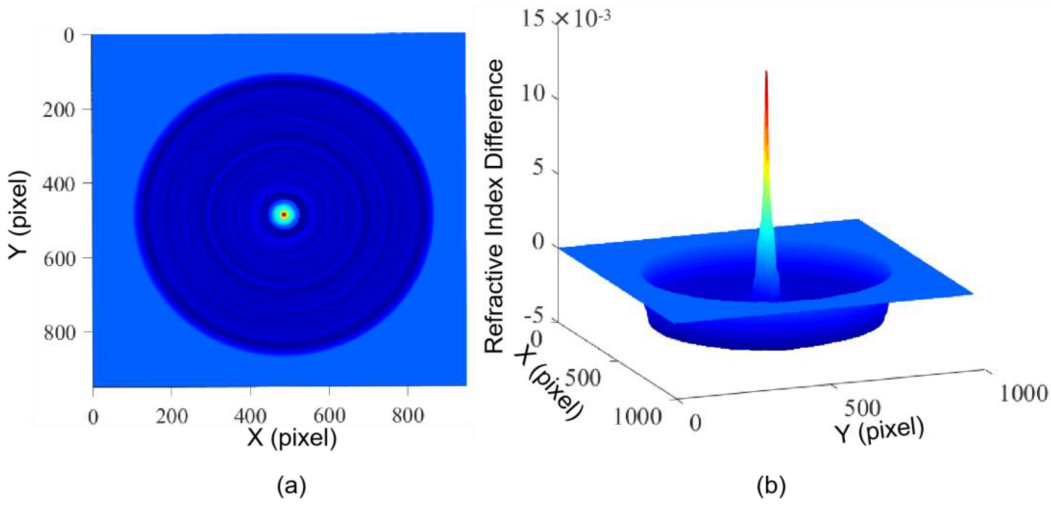

Fig. 10. (a)Two-dimensional RI difference diagram of the fiber cross-section; (b) three-dimensional RI distribution of fiber.

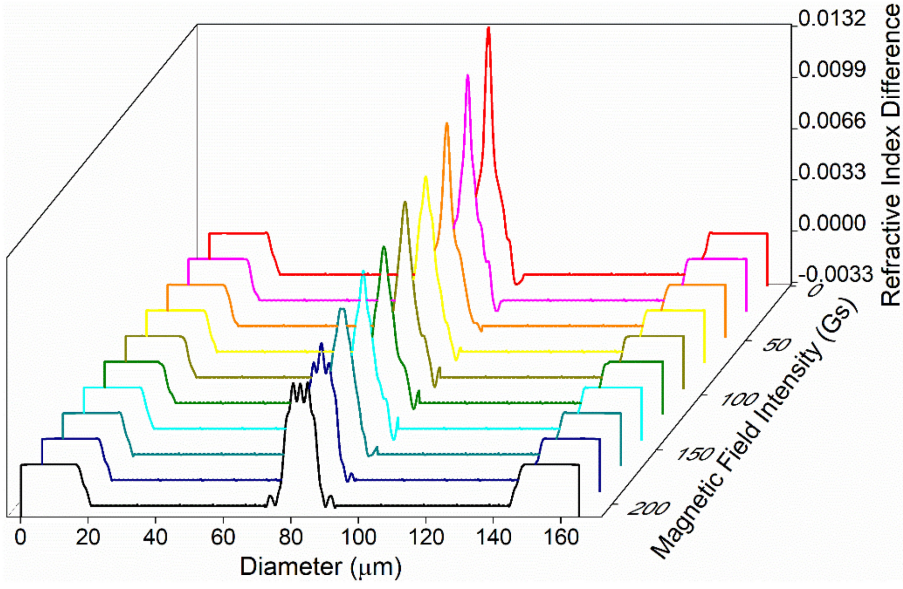

Fig. 11. RI distribution curve of EYDF in different magnetic fields.

field intensity increased from 0 to 250 Gs, the RI of the SMF remained almost constant. In contrast, the RIC in the core doped with Er and Yb was evident, decreasing from 0.0162 to 0.0081. The sensitivity, which is the ratio of RIC to magnetic field change dn/dGs, reached above 3.8279×10^{-5} RIU/Gs with the R^2 value of 0.9888.

The PPMS experiment demonstrates that under the action of an external magnetic field, the magnetic moment and magnetic susceptibility of EYDF change significantly; the magnetic susceptibility decreases with an increase of the magnetic field. Theoretical calculations show that because the magnetic field changes the magnetic susceptibility and RI of the optical fiber, the experimental RIC of EYDF decreases with an increase in the magnetic field. The experimental results are consistent with the theory. Theoretical calculations also show that the RIC is closely related to the magnetic

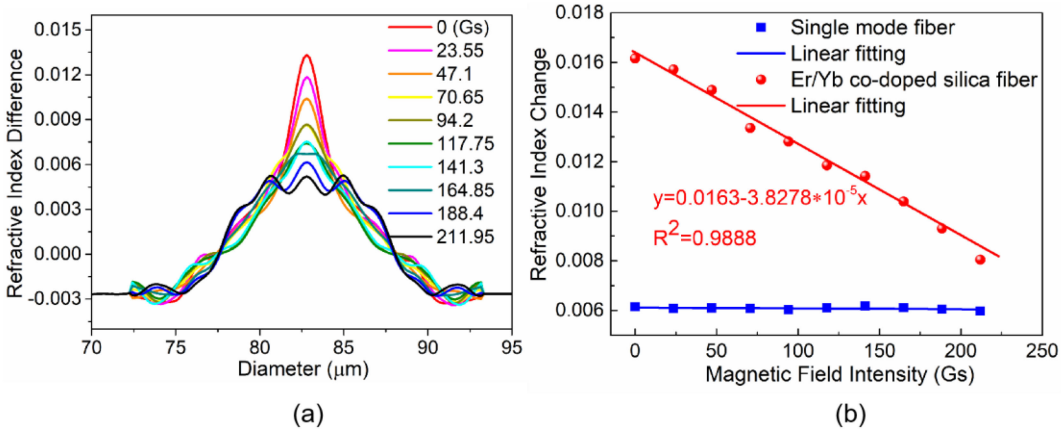

Fig. 12. (a) RI distribution curve of EYDF core in different magnetic fields. (b)Relationship between the RIC and magnetic field intensity in the range 0 - 250 Gs.

moments and 4f unpaired spin electrons of the Er and Yb atoms. There is a strong interaction between the rare-earth spintronics and the silicon ring, and it is easily polarized under an external magnetic field. Additionally, it appears as a change in RI macroscopically, which systematically explains the mechanism of the magnetic refractive effect of the EYDF.

4. Conclusion

In this study, we established the geometrical structure of EYDF-3MR, and calculated its spin density and electron structure using DFT. The results show that there is a strong interaction between the 4f electrons of Er and Yb atoms and the 2p electrons of the O atom of silicon dioxide through the conduction of 6s electrons in the outer layer of the Er and Yb atoms. The Er and Yb atoms are responsible for the main contribution to the spin characteristics and electron transfer in the optical fiber model. The experimental investigation of the of the measurement system of the optical fiber RIC was realized based on the digital hologram technique and obtained the magnetic field dependence of 2D and 3D RI curves. The results show that the RIC of the core doped with Er/Yb is evident, decreasing from 0.0162 to 0.0081 as the magnetic field intensity increases from 0 to 250 Gs. The sensitivity of the RIC of the EYDF can reach 3.8279×10^{-5} RIU/Gs and is two orders of magnitude higher than that of the SMF. In addition, the experiment results are consistent with the theory and provide that the sensitivity of the magneto-refractive fiber improves significantly upon doping with rear-earth element. This may provide important insights into the design of rare-earth-doped optical fibers and the practical application of potential magnetic field sensors.

References

[1] J. Lenz and A. S. Edelstein, "Magnetic sensors and their applications," *IEEE Sensors J.*, vol. 6, no. 3, pp. 631–649, Jun. 2006.
[2] F. Hou, *et al.*, "Magnetic fluid infiltrated microbottle resonator sensor with axial confined mode," *IEEE Photon. J.*, vol. 12, no. 5, Oct. 2020, Art. no. 6802709.
[3] Y. Huang, H. Chen, W. Dong, F. Pang, J. Wen, Z. Chen, and T. Wang, "Fabrication of europium-doped silica optical fiber with high Verdet constant," *Opt. Exp.*, vol. 24, no. 16, pp. 18709–18717, 2016.
[4] Y. Zhao, D. Wu, R. Q. Lv, and Y. Ying, "Tunable characteristics and mechanism analysis of the magnetic fluid refractive index with applied magnetic field," *IEEE Trans. Magn.*, vol. 50, no. 8, pp. 1–5, Aug. 2014.
[5] A. H. Reid, *et al.*, "Beyond a phenomenological description of magnetostriction," *Nature Commun.*, vol. 9, no. 1, 2018, Art. no. 388.
[6] Y. Zhou, Y. Zhao, D. Zhang, X. Shu, and S. Che, "A new optical method for suppressing radial magnetic error in a depolarized interference fiber optic gyroscope," *Sci. Rep.*, vol. 8, no. 1, 2018, Art. no. 1972.

[7] L. Luo, S. Pu, S. Dong, and J. Tang, "Fiber-optic magnetic field sensor using magnetic fluid as the cladding," *Sensor Actuat. A-Phys.*, vol. 236, pp. 67–72, 2015.
[8] Y. Zheng, L. H. Chen, J. Yang, R. Raghunandhan, X. Dong, P. L. So, and C. C. Chan, "Fiber optic fabry–perot optofluidic sensor with a focused ion beam ablated microslot for fast refractive index and magnetic field measurement," *IEEE J. Sel. Topics Quantum. Electron.*, vol. 23, no. 2, pp. 322–326, Mar./Apr. 2017.
[9] H. Tian, Y. Song, Y. Li, and H. Li, "Fiber-optic vector magnetic field sensor based on mode interference and magnetic fluid in a two-channel tapered structure," *IEEE Photon. J.*, vol. 11, no. 6, Dec. 2019, Art. no. 7104309.
[10] N. Alberto, M. F. Domingues, C. Marques, P. Andre, and P. Antunes, "Optical fiber magnetic field sensors based on magnetic fluid: A review," *Sensors (Basel)*, vol. 18, no. 12, 2018, Art. no. 4325.
[11] B. Wu, *et al.*, "Magnetic field sensor based on a dual-frequency optoelectronic oscillator using cascaded magnetostrictive alloy-fiber Bragg grating-Fabry Perot and fiber Bragg grating-Fabry Perot filters," *Opt. Expr.*, vol. 26, no. 21, pp. 27628–27638, 2018.
[12] J. F. Herbst, R. E. Watson, and J. W. Wilkins, "Relativistic calculations of 4f excitation energies in the rare-earth metals: Further results," *Phys. Rev. B*, vol. 17, no. 8, pp. 3089–3098, 1978.
[13] Q. Wang, J. Wen, Y. Luo, G. Peng, F. Pang, Z. Chen, and T. Wang, "Enhancement of lifetime in Er-doped silica optical fiber by doping Yb ions via atomic layer deposition," *Opt. Mater. Exp.,* vol. 10, no. 2, pp. 397–407, 2020.
[14] S. A. Umar, M. K. Halimah, K. T. Chan, and A. A. Latif, "Polarizability, optical basicity and electric susceptibility of Er^{3+} doped silicate borotellurite glasses," *J. Non-Cryst. Solids*, vol. 471, pp. 101–109, 2017.
[15] V. P. Danilov, A. M. Prokhorov, M. I. Studenikin, D. Schmid, L. O. Schwan, and R. Glasmacher, "Concentration quenching of luminescence from the $^2P_{3/2}$ level of Er^{3+} ion in $Y_3Al_5O_{12}$ and $YAlO_3$ crystals," *Phys. Statist. Solidi*, vol. 177, no. 2, pp. 593–600, 2000.
[16] S. Datta, C. T. Chan, K. M. Ho, and C. M. Soukoulis, "Effective dielectric constant of periodic composite structures," *Phys. Rev. B: Condens. Matter.,* vol. 48, no. 20, pp. 14936–14943, 1993.
[17] P. P. Pradyumnan, C. Joseph, and M. A. Ittyachen, "Magnetic moment and susceptibility measurement studies of double rare earth hydrogen selenite crystals," *J. Magn. Magn. Mater.*, vol. 202, pp. 493–496, 1999.
[18] S. Paranthaman, J. Moon, J. Kim, D. E. Kim, and T. K. Kim, "Performance of density functional theory and relativistic effective core potential for Ru-based organometallic complexes," *J. Phys. Chem. A*, vol. 120, no. 13, pp. 2128–34, 2016.
[19] K. F. Garrity, J. W. Bennett, K. M. Rabe, and D. Vanderbilt, "Pseudopotentials for high-throughput DFT calculations," *Comput. Mater. Sci.*, vol. 81, pp. 446–452, 2014.
[20] T. Y. Wang, J. X. Wen, W. Y. Luo, Z. Y. Xiao, and Z. Y. Chen, "Influences of irradiation on network microstructure of low water peak optical fiber material," *J. Non-Cryst. Solids*, vol. 356, no. 25-27, pp. 1332–1336, 2010.
[21] M. J. Frisch, *et al.*, "Gaussian 09, revision D. 01,Gaussian, Inc. Wallingford CT," 2013.
[22] T. Lu and F. Chen, "Multiwfn: A multifunctional wavefunction analyzer," *J. Comput. Chem.*, vol. 33, no. 5, pp. 580–92, 2012.
[23] R. Hanna, "Infrared absorption spectrum of silicon dioxide," *J. Amer. Ceramic Soc.*, vol. 48, no. 11, pp. 595–599, 1965.
[24] W. M. M. Sitarz and M. Handke, "Rings in the structure of silicate glasses," *J. Mol. Struct.*, vol. 511, pp. 281–285, 1996.
[25] M. F. F. Rocca, A. Kuzmin, N. Daldosso, C. Duverger, and F. Monti, "EXAFS studies of the local structure of Er^{3+} ions in silica xerogels co-doped with aluminium," *J. Non-Cryst. Solids*, vol. 293–295, pp. 112–117, 2001.
[26] P. Ke, K. Yue, Z. You, W. Luo, Q. Guo, and J. Wen, "Investigation on structure and luminescence properties of Yb^{3+}-doped silica materials," *Modell. Simul. Mater. Sci. Eng.*, vol. 28, no. 1, 2020.
[27] M. Xin, X. Dai, J. Han, M. Jin, C. A. Jimenez-Cruz, D. Ding, Z. Wang, and R. Zhou, "Carbon nanotubes adsorb U atoms differently in their inner and outer surfaces," *RSC Adv.*, vol. 4, no. 57, pp. 30074–30080, 2014.
[28] C. Kalaiarasi *et al.*, "Investigation of bond topological and electrostatic properties of plumbagin molecule: An experimental and theoretical charge density study," *J. Mol. Struct.*, vol. 1220, 2020, Art. no. 128714.
[29] A. E. Reed, R. B. Weinstock, and F. Weinhold, "Natural population analysis," *J. Chem. Phys.*, vol. 83, no. 2, pp. 735–746, 1985.
[30] C. Yan, S. Huang, Z. Miao, Z. Chang, J. Zeng, and T. Wang, "3D refractive index measurements of special optical fibers," *Opt. Fiber Technol.*, vol. 31, pp. 65–73, 2016.
[31] S. Huang, W. Wang, J. Zeng, C. Yan, Y. Lin, and T. Wang, "Measurement of the refractive index of solutions based on digital holographic microscopy," *J. Opt.*, vol. 20, no. 1, 2018, Art. no. 015704.